

A new magnitude–redshift relation based on Type Ia supernovae

Ósmar Rodríguez^{1,2,*} and Alejandro Clocchiatti^{1,2}

¹ Pontificia Universidad Católica de Chile, Vicuña Mackenna, 4860 Macul, Santiago, Chile

² Instituto Milenio de Astrofísica (MAS), Nuncio Monseñor Sótero Sanz 100, Of. 104, Santiago, Chile

Received 13 January 2026 / Accepted 2 March 2026

ABSTRACT

We present a new empirical relation between the standardised magnitude (m) of Type Ia supernovae (SNe Ia) and redshift (z). Using the Pantheon+ sample and the Dark Energy Survey (DES) five-year sample (DES-SN5YR), we find a negative linear correlation between $m - 5 \log(z(1+z))$ and z , implying that their magnitude–redshift relation can be parametrised with just two parameters: an intercept \mathcal{M} and a slope b . This relation corresponds to the luminosity distance $d_L(z) = c H_0^{-1} z(1+z) 10^{bz/5}$ and is valid up to at least $z \simeq 1.1$. It outperforms the Λ CDM and flat w CDM models and the (2,1) Padé approximant for $d_L(z)$, and performs comparably to the flat Λ CDM model and the (2,1) Padé ($j_0 = 1$) model of Hu et al. Furthermore, the relation is relatively stable in the absence of low- z SNe, making it suitable for fitting Hubble diagrams of SNe Ia without adding a low- z sample. In deep fields, assuming that the large-scale density is independent of the comoving radial coordinate, $b \propto q_0 + 1$. We fitted the empirical relation to Hubble diagrams of eight deep-field regions and find no evidence for anisotropy. The inferred q_0 values, ranging from -0.6 to -0.4 , are consistent within 1.6σ and significantly lower than zero, indicating statistically consistent cosmic acceleration across all eight regions. We applied the empirical relation to the DES-Dovekie and Amalgame SN samples and find b values consistent with those from DES-SN5YR and Pantheon+. Finally, using the empirical relation in the hemispheric comparison method applied to Pantheon+ up to $z = 1.1$, we find no evidence for anisotropies in \mathcal{M} and b .

Key words. supernovae: general – cosmological parameters – cosmology: theory

1. Introduction

General relativity and the assumption of homogeneity and isotropy of the Universe at large scales are two of the foundations of modern cosmology. The latter leads to the Friedmann–Lemaître–Robertson–Walker (FLRW) metric, under which Einstein’s field equations reduce to the Friedmann equations. The first, combined with the FLRW metric, provides a formula for the luminosity distance–redshift relation, $d_L(z)$, in terms of three parameters: the Hubble constant (H_0), the matter density (Ω_M), and the cosmological constant (Λ) with density parameter Ω_Λ .

Using Hubble diagrams of Type Ia supernovae (SNe Ia), Riess et al. (1998) and Perlmutter et al. (1999) found $\Omega_\Lambda > 0$ and a deceleration parameter $q_0 < 0$, indicating that the Universe’s expansion is currently accelerating. In this context, Λ is interpreted as a constant dark energy density that drives cosmic acceleration. Given that models with Λ , when fitted to various observational data, yield $\Omega_\Lambda > 0$ (Weinberg et al. 2013), the existence of dark energy is widely accepted, consolidating the Λ cold dark matter (Λ CDM) model as the standard model.

Despite its ability to fit observations, the Λ CDM model has problems of fine-tuning, cosmic coincidence, and tensions in cosmological parameters measured with independent experiments (Perivolaropoulos & Skara 2022; Efstathiou 2025). These issues motivate alternative gravitational theories that explain cosmic acceleration without Λ (Koyama 2016; Odintsov et al. 2025). Moreover, cosmic acceleration may be partly an apparent effect associated with the assumption of homogeneity and isotropy and the corresponding use of the FLRW metric (Räsänen 2006; Enqvist 2008; Wiltshire 2009).

Cosmography provides a model-independent framework to study cosmic acceleration, expressing $d_L(z)$ in terms of spatial

curvature and kinematic parameters, such as H_0 , q_0 , and the jerk parameter (j_0). However, this approach relies on the assumption of a homogeneous and isotropic Universe (Hu & Wang 2022).

Among current SN Ia samples, such as Pantheon+ (Brout et al. 2022) and the full five-year sample from the Dark Energy Survey Supernova (DES-SN) program (DES-SN5YR; Sánchez et al. 2024), a significant fraction of SNe originates from deep-field surveys. Analysing deep fields separately allows one to infer direction-dependent parameters without requiring global homogeneity and isotropy. In particular, comparing deep fields across different directions provides a test of isotropy.

Since angular variations in deep fields are expected to be negligible, and assuming that the large-scale density within each field is independent of the comoving radial coordinate, the metric can be approximated as FLRW on a field-by-field basis. Under this assumption, we can measure q_0 for each deep field using the FLRW metric, without assuming global homogeneity and isotropy. The main limitation of this approach is the small number of low- z SNe Ia ($z < 0.1$) in deep fields, which are crucial for breaking parameter degeneracies (Linder 2006).

An approach to reducing the impact of the lack of low- z SNe on the estimation of q_0 is to use a $d_L(z)$ relation with as few parameters as possible. In the flat Λ CDM model, $d_L(z)$ depends only on H_0 and Ω_M . The latter, which is used to measure q_0 , remains relatively stable in the absence of low- z SNe (Brout et al. 2022). To date, the only other $d_L(z)$ relation that accurately fits SN observations with just two parameters is that proposed by Hu et al. (2024a). This relation corresponds to a third-order Padé approximation with H_0 and q_0 as free parameters, while j_0 is fixed to one, as predicted by the flat Λ CDM model (Bochner et al. 2015).

In this work, we introduce an empirical magnitude–redshift relation ($m(z)$) and the corresponding $d_L(z)$ relation, which

* Corresponding author: olrodrig@gmail.com

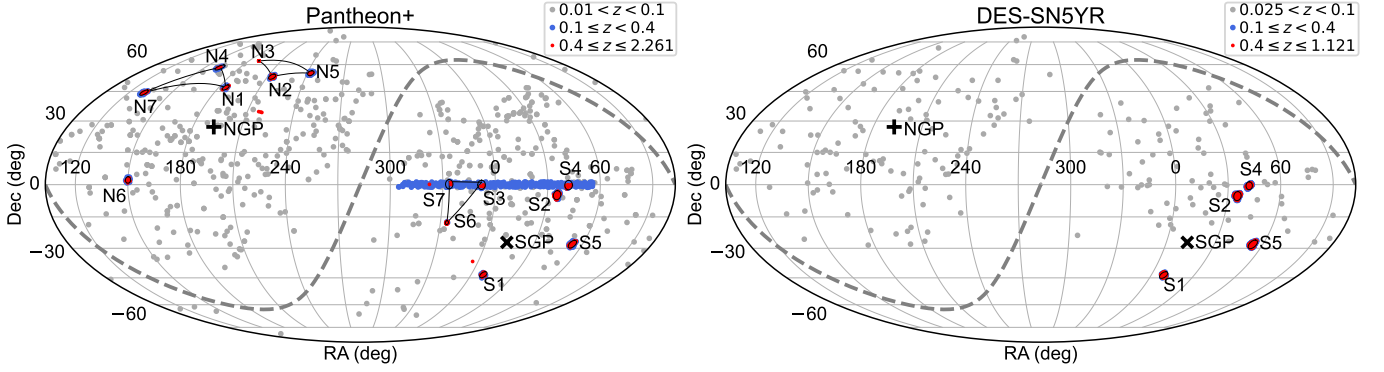


Fig. 1. Sky distribution of Pantheon+ and DES-SN5YR SNe. Dashed lines indicate the Galactic equator. Plus and cross symbols mark the north and south Galactic poles, respectively. Circular and triangular regions are also shown.

provides a straightforward quantitative tool to fit Hubble diagrams of SNe Ia up to at least $z \simeq 1.1$, using only two parameters and without assuming any theoretical model or spatial curvature. This relation is relatively stable in the absence of low- z SNe, making it suitable for studying SN deep fields without the need to add a low- z sample.

The paper is organised as follows. In Sect. 2, we describe the SN samples and define the deep-field regions. In Sect. 3, we present the $m(z)$ relations used to fit Hubble diagrams. In Sect. 4, we present the results, including the new empirical relation, its comparison with five $m(z)$ relations, and its application to the deep-field regions and other samples. In Sect. 5, we discuss the derived j_0 values, the search for cosmic anisotropies, and future analyses. We summarise our conclusions in Sect. 6.

2. Data samples

Pantheon+¹ contains data from 1550 SNe Ia, drawn from 18 surveys, with $0.001 \leq z \leq 2.261$. DES-SN5YR² contains data from 1635 photometrically classified SNe Ia from the DES-SN programme with $0.060 \leq z \leq 1.121$, and 194 SNe Ia from four surveys with $0.025 < z < 0.093$, referred to as the low- z sample.

The Pantheon+ and DES-SN5YR samples provide (i) RA and Dec coordinates; (ii) standardised SN magnitudes (m_B^{corr} , hereafter m), derived from SALT2 (Pantheon+) and SALT3 (DES-SN5YR) light-curve fits and corrected for stretch, colour, host-galaxy mass, and selection bias; (iii) redshifts corrected for the cosmic microwave background (CMB) dipole and peculiar velocities (z_{HD} , hereafter z); and (iv) the covariance matrix (\mathbf{C}) to account for statistical and systematic errors.

Following Brout et al. (2022), we selected SNe with $z > 0.01$ from the Pantheon+ compilation to minimise the impact of peculiar velocities on the derived cosmological parameters. We refer to this subsample as Pantheon+. Because DES-SN5YR introduced several improvements compared with Pantheon+, its m values are not on the same scale. Specifically, there is a constant offset of 0.04 mag between the selection bias corrections in DES-SN5YR and Pantheon+, which does not affect the cosmological results of each separate analysis (Vincenzi et al. 2025). Hence, we analysed both samples separately.

Fig. 1 shows the sky distribution of SNe in Pantheon+ and DES-SN5YR. The SNe with $z \geq 0.4$ are concentrated in small regions of the sky, which reflects the location of the SN deep fields. We defined 14 circular regions for Pantheon+ and four

for DES-SN5YR, referred to as XY, which contain virtually all SNe with $z \geq 0.4$. In this notation, X denotes the closest Galactic pole and Y indicates the rank of proximity to that pole. Table 1 lists the regions, their centres in (RA, Dec), angular radii (θ), the number of SNe within each region, and the corresponding z ranges.

The S1, S2, S4, and S5 regions in Pantheon+ closely match those in DES-SN5YR. In these regions, DES-SN5YR contains 170–490 more SNe than Pantheon+, while 47–100% of the SNe in the Pantheon+ S1, S2, S4, and S5 regions originate from the DES-SN programme and are already included in DES-SN5YR. Therefore, we used only the DES-SN5YR data for these regions.

The remaining ten Pantheon+ regions contain 13–77 SNe each. To increase the sample while minimising the sky area, we defined the triangular N147, N235, and S367 regions. The N147 region includes N1, N4, N7, and the SNe located within the triangle formed by their centres; the same applies for N235 and S367. For S367, we increased the declination of the centres of S3 and S7 by 1.2° to include more SNe without significantly increasing the area. Fig. 1 shows the triangular regions, while Table 1 lists their barycentres, the number of SNe, and the z ranges. We refer to the S1, S2, S4, S5, N147, N235, S367, and N6 regions as the deep-field regions.

3. Methods

3.1. Magnitude–redshift relations

The $m(z)$ relation for a standard candle with absolute magnitude M is given by

$$m(z) = M + 5 \log \mathcal{D}_L(z), \quad (1)$$

where $M = M + 5 \log(c H_0^{-1} \text{Mpc}^{-1}) + 25$ and $\mathcal{D}_L(z) = d_L(z) H_0 / c$. To derive $d_L(z)$ using either a gravitational theory or a cosmographic expansion, we need the metric of the expanding Universe. The simplest choice is the FLRW metric, characterised by the scale factor a and the curvature parameter k . For this metric,

$$d_L(z) = (1+z)d_M(z), \quad (2)$$

where $d_M(z)$ is the transverse comoving distance. Defining $H(z) = \dot{a}/a$ and $\Omega_k = -kc^2/H_0^2$, $d_M(z)$ is given by

$$d_M(z) = \frac{c}{H_0} \begin{cases} \Omega_k^{-1/2} \sinh(\Omega_k^{1/2} \int_0^z \frac{H_0}{H(z')} dz') & \Omega_k > 0 \\ \int_0^z \frac{H_0}{H(z')} dz' & \Omega_k = 0 \\ |\Omega_k|^{-1/2} \sin(|\Omega_k|^{1/2} \int_0^z \frac{H_0}{H(z')} dz') & \Omega_k < 0 \end{cases} \quad (3)$$

¹ <https://github.com/PantheonPlusSH0ES/DataRelease>

² <https://doi.org/10.5281/zenodo.12720778>

Table 1. Supernova regions.

Region	RA (°)	Dec (°)	θ (°)	z range	#SNe
Pantheon+					
S1	8.57	-43.36	1.60	0.148–0.609	34
S2	35.56	-4.88	2.12	0.017–1.912	134
S3	352.15	-0.09	2.17	0.079–0.508	34
S4	41.89	-0.21	2.19	0.134–0.638	57
S5	53.78	-28.00	1.89	0.103–1.549	97
S6	333.83	-17.70	0.61	0.371–0.789	44
S7	333.68	0.20	2.14	0.040–0.419	43
N1	185.14	47.10	1.37	0.025–0.545	24
N2	213.64	53.01	1.47	0.082–1.615	64
N3	189.24	62.22	0.10	0.840–2.261	13
N4	162.85	58.30	1.52	0.023–0.503	20
N5	242.82	54.96	1.40	0.122–0.576	30
N6	150.05	2.18	1.51	0.047–1.543	77
N7	130.55	44.39	1.44	0.071–0.578	37
S367	339.96	-5.10	–	0.015–0.789	163
N147	158.83	52.31	–	0.023–0.578	89
N235	216.91	58.56	–	0.082–2.261	107
DES-SN5YR					
S1	8.63	-43.53	1.76	0.073–0.818	295
S2	35.57	-5.32	2.11	0.138–1.044	518
S4	42.00	-0.51	1.83	0.094–0.733	231
S5	53.83	-28.09	2.11	0.060–1.121	591

3.1.1. The Λ CDM, flat Λ CDM, and flat w CDM models

In the phenomenological generalisation of the Λ CDM model,

$$H(z) = H_0 \sqrt{\Omega_M(1+z)^3 + \Omega_k(1+z)^2 + \Omega_\Lambda(1+z)^{3(1+w)}}, \quad (4)$$

where $\Omega_M + \Omega_\Lambda + \Omega_k = 1$ and w is the dark energy equation-of-state parameter. We used the $m(z)$ relations for Λ CDM ($w = -1$), flat Λ CDM ($\Omega_k = 0$, $w = -1$), and the phenomenological flat w CDM ($\Omega_k = 0$) models.

3.1.2. Padé cosmography and flat Padé model

The Padé approximation is a method to approximate a function $F(z)$ as the ratio of two polynomials of orders A and B . The rational function is known as the (A,B) Padé approximant, and its coefficients are expressed in terms of those of the Taylor series of $F(z)$ truncated at order $A + B$ (Baker & Graves-Morris 1996).

Hu & Wang (2022), using Pantheon (Scolnic et al. 2018), report that the (2,1) Padé approximant for $d_L(z)$ performs better than cosmographic expansions based on Taylor series. More recently, Hu et al. (2024a) analysed Pantheon+ and found that this approximant outperforms other Padé forms. We therefore adopt it as the best cosmographic approach.

The (2,1) Padé approximant for $d_L(z)$ used by Hu et al. (2024a) was derived by Capozziello et al. (2020) for $\Omega_k = 0$. To compute the expression valid for any Ω_k , we used the third-order Taylor series for $d_L(z)$ (Eq. 2 of Cattoën & Visser 2007) and the procedure of Baker & Graves-Morris (1996), obtaining

$$d_L(z) = \frac{cz}{H_0} \frac{6(1-q_0) + (5-8q_0-3q_0^2+2\hat{j}_0)z}{6(1-q_0) + 2(1-q_0-3q_0^2+\hat{j}_0)z}. \quad (5)$$

Here, $\hat{j}_0 \equiv j_0 - \Omega_k$, and

$$q_0 = \left. \frac{d \ln H(z)}{dz} \right|_{z=0} - 1, \quad j_0 = \left. \frac{1}{H_0} \frac{d^2 H(z)}{dz^2} \right|_{z=0} + q_0^2. \quad (6)$$

For $\Omega_k = 0$, Eq. (5) is equivalent to that given in Hu et al. (2024a). We refer to Eq. (5) as the Padé cosmography.

Hu et al. (2024a) also found that the (2,1) Padé approximant for $d_L(z)$ with $j_0 = 1$ fixed performs better than the Padé cosmography, the flat Λ CDM, Λ CDM, and flat w CDM models. Since j_0 was fixed to unity because this is the value for the flat Λ CDM model, the $d_L(z)$ equation proposed by Hu et al. (2024a) is not cosmographic, but rather model-based. We refer to Eq. (5) assuming $\hat{j}_0 = 1$ as the flat Padé model.

3.1.3. Empirical approach

To fit the Hubble diagram, we introduce the ansatz

$$d_L(z) = \frac{cz}{H_0} (1+z) 10^{f(z)/5}, \quad (7)$$

where the factor $1+z$ is inspired by Eq. (2) and $f(z)$ is a free function that vanishes as $z \rightarrow 0$, ensuring $d_L(z) = cz/H_0$ at low z . The corresponding $m(z)$ relation is

$$m(z) = \mathcal{M} + 5 \log(z(1+z)) + f(z), \quad (8)$$

where the dependence of $f(z)$ on z can be empirically determined from the correlation between $m - 5 \log(z(1+z))$ and z .

3.2. Parameter estimation and model selection

Let \mathbf{v} denote the vector with the n_p free parameters of $m(z)$. The posterior probability of $m(z)$ is $P \propto p(\mathbf{v}) \mathcal{L}$, where $p(\mathbf{v})$ is the prior and $\mathcal{L} = e^{-\chi^2/2}$. Following Conley et al. (2011),

$$\chi^2 = \Delta \mathbf{m}^T \mathbf{C}^{-1} \Delta \mathbf{m}, \quad (9)$$

where $\Delta \mathbf{m}$ is the vector of residuals, whose i -th component is

$$\Delta m_i = m_i - m(z_i, \mathbf{v}). \quad (10)$$

We assumed non-informative priors; in this case, we obtained the best-fit parameter vector \mathbf{v}_{best} that maximises P by minimising χ^2 .

To calculate uncertainties, we used EMCEE (Foreman-Mackey et al. 2013), which samples P using a Markov chain Monte Carlo (MCMC) process. First, we defined the priors as flat distributions: $\mathcal{M} \in (23, 25)$, $\Omega_M \in (0, 1)$, $\Omega_\Lambda \in (0, 1)$, $w \in (-2, 0)$, $q_0 \in (-2, 1)$, and $\hat{j}_0 \in (-4, 7)$. These priors are wide enough to consider them as uninformative. Next, we initialised $10n_p$ walkers in a small Gaussian ball around \mathbf{v}_{best} and ran 10^5 steps (10^6 for the flat w CDM model). Then, given an integrated autocorrelation time (τ) provided by EMCEE, we discarded the initial 3τ steps as burn-in and thin by $\tau/2$. With this configuration, we obtain for all parameters a Gelman & Rubin (1992) statistic of $\hat{R} \approx 1.0$, indicating convergence of the MCMC chains, and an effective sample size $n_{\text{eff}} > 2000$ ($n_{\text{eff}} > 400$ for the flat w CDM model). Finally, for each parameter, we adopted the 68.27% confidence interval of its marginalised distribution as the 1σ uncertainty.

To identify which model among a set of candidates best describes the Hubble diagram, we used the corrected Akaike information criterion (AICc; Sugiura 1978) and the Bayesian information criterion (BIC; Schwarz 1978). For each model, we computed $\text{AICc} = \chi_{\text{min}}^2 + 2n_p N / (N - n_p - 1)$ and $\text{BIC} = \chi_{\text{min}}^2 + n_p \ln N$, where $\chi_{\text{min}}^2 = \chi^2(\mathbf{v}_{\text{best}})$ and N is the number of SNe. Based on these information criteria (ICs), the preferred model is the one with the lowest IC value (IC_{min}), and the strength of evidence for each model is given by $\Delta \text{IC} = \text{IC} - \text{IC}_{\text{min}}$. Models

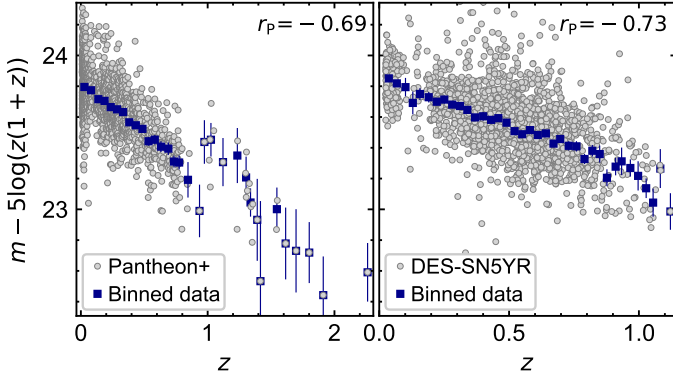


Fig. 2. Relation between $m - 5 \log(z(1+z))$ and z for Pantheon+ and DES-SN5YR. Binned data (blue squares) with error bars are shown for visualisation purposes only, both here and throughout the paper.

with $\Delta_{\text{AICc}} < 2$ have substantial support, while those with $4 < \Delta_{\text{AICc}} < 7$ have considerably less support (Burnham & Anderson 2002). Similarly, $\Delta_{\text{BIC}} < 2$ indicates little evidence against the model, and $6 < \Delta_{\text{BIC}} < 10$ indicates strong evidence against the model (Kass & Raftery 1995). Therefore, models with both $\Delta_{\text{AICc}} < 2$ and $\Delta_{\text{BIC}} < 2$ perform comparably, yielding similar fits to the Hubble diagram. Models with larger Δ_{AICc} are progressively less supported, and those with larger Δ_{BIC} are increasingly disfavoured.

4. Results

4.1. Empirical relation

Figure 2 shows $m - 5 \log(z(1+z))$ versus z for Pantheon+ and DES-SN5YR. Their weighted Pearson correlation coefficients (r_p ; Earp et al. 2019) are close to -0.7 , with p -values below 10^{-220} , indicating a moderate-to-strong negative linear correlation. Based on this, we express $m - 5 \log(z(1+z))$ as a linear function of z , with an intercept \mathcal{M} and a slope b :

$$m(z) = \mathcal{M} + bz + 5 \log(z(1+z)). \quad (11)$$

Thus, $f(z) = bz$ in Eq. (8), which, together with Eq. (7) yields

$$d_L(z) = \frac{cz}{H_0} (1+z) 10^{bz/5}. \quad (12)$$

We refer to Eqs. (11) and (12) as the empirical relation.

The empirical relation exhibits several characteristics. First, it is relatively stable in the absence of low- z SNe (see Sect. 4.5). Second, its parameters and their associated covariance matrix can be computed analytically. Fig. 3 shows the confidence contours for \mathcal{M} and b computed analytically and using EMCEE (using the flat prior $b \in (-2, 0)$), which are virtually identical. Third, under the FLRW metric, $b \propto q_0 + 1$. Indeed, from Eqs. (12) and (2),

$$d_M(z) = \frac{cz}{H_0} 10^{bz/5}, \quad (13)$$

and using Eq. (16) of Li et al. (2020),

$$H(z) = H_0 \frac{\sqrt{10^{-2bz/5} + \Omega_k z^2}}{1 + b \ln(10)z/5}, \quad (14)$$

which, together with Eq. (6), yields

$$q_0 = -\frac{2}{5} \ln(10)b - 1. \quad (15)$$

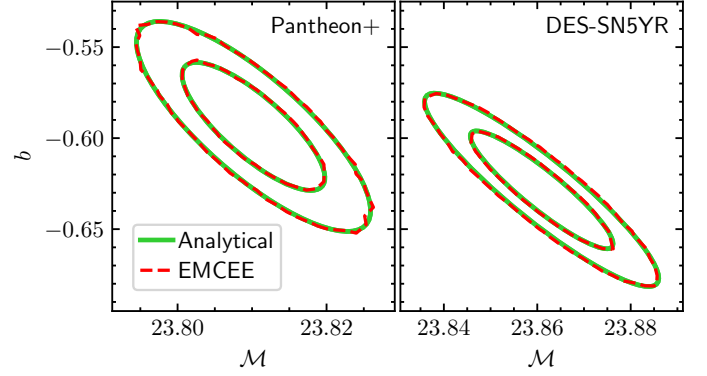


Fig. 3. Confidence contours at the 68.27% and 95.45% levels of the empirical relation parameters, obtained analytically and using EMCEE.

4.2. Constraints on cosmological parameters

Table 2 lists the parameter constraints from Pantheon+ and DES-SN5YR for the six $m(z)$ relations used in this work. The parameters for the flat Λ CDM, Λ CDM, and flat w CDM models are consistent with those reported by the Pantheon+ team ($\Omega_M = 0.334 \pm 0.018$ for the flat Λ CDM model, $\Omega_M = 0.306 \pm 0.057$ and $\Omega_\Lambda = 0.625 \pm 0.084$ for the Λ CDM model, and $\Omega_M = 0.309^{+0.063}_{-0.069}$ and $w = -0.90 \pm 0.14$ for the flat w CDM model; Brout et al. 2022) and the DES Collaboration ($\Omega_M = 0.352 \pm 0.017$ for the flat Λ CDM model, $\Omega_M = 0.291^{+0.063}_{-0.065}$ and $\Omega_\Lambda = 0.55 \pm 0.10$ for the Λ CDM model, and $\Omega_M = 0.264^{+0.074}_{-0.096}$ and $w = -0.80^{+0.14}_{-0.16}$ for the flat w CDM model; Camilleri et al. 2024).

For each $m(z)$ relation, the parameters derived from DES-SN5YR and Pantheon+ are consistent within 1σ , except for \mathcal{M} , which differs by more than 3.3σ . This discrepancy arises from the constant offset of 0.04 mag between selection bias corrections in DES-SN5YR and Pantheon+ (Vincenzi et al. 2025). After accounting for this offset, the \mathcal{M} values derived from DES-SN5YR and Pantheon+ become consistent within 1σ .

4.3. Hubble diagrams and model comparison

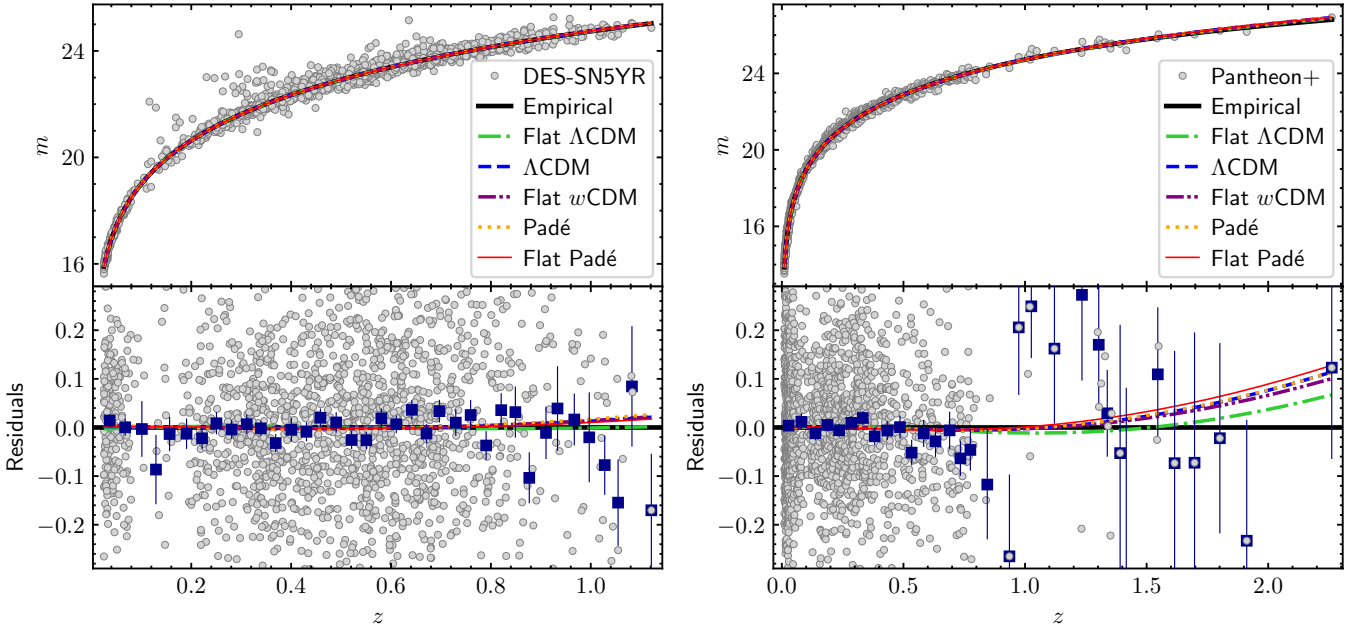
Fig. 4 shows the Hubble diagrams for DES-SN5YR and Pantheon+, the best fits for the $m(z)$ relations, and the residuals relative to the empirical relation. For DES-SN5YR, the empirical relation provides a fit comparable to the other $m(z)$ relations. The differences between the $m(z)$ relations and the empirical relation have rms values below 0.009 mag and maximum absolute deviations Δm_{max} below 0.027 mag. For Pantheon+, the empirical relation begins to diverge from the other $m(z)$ relations at $z \gtrsim 1.4$. For $z < 1.121$ (the highest z in DES-SN5YR), the rms and Δm_{max} remain below 0.007 and 0.012 mag, respectively.

Given that the empirical relation accurately reproduces the Hubble diagrams of both samples up to $z = 1.121$, we assume that it is valid at least up to this redshift. Beyond this limit, we cannot reliably assess its validity because Pantheon+ contains only 19 SNe at $z > 1.121$. In the following, we restrict our analyses of Pantheon+, including its deep-field regions, to $z < 1.121$, although analyses without this cut lead to the same conclusions. Table 2 lists the parameter constraints for Pantheon+ ($z < 1.121$).

Table 3 lists the Δ_{AICc} and Δ_{BIC} values. Based on these values, the empirical relation, the flat Λ CDM model, and the flat Padé model provide comparable fits to the Hubble diagrams of DES-SN5YR and Pantheon+ ($z < 1.121$), with the flat Λ CDM model being only marginally disfavoured for

Table 2. Parameter constraints for different magnitude–redshift relations.

Relation	M	b	Ω_M	Ω_Λ	w	q_0	\hat{f}_0
DES-SN5YR							
Empirical	23.861 ± 0.010	-0.628 ± 0.021	–	–	–	–	–
Flat Λ CDM	23.857 ± 0.011	–	0.350 ± 0.017	–	–	–	–
Λ CDM	23.863 ± 0.013	–	$0.297^{+0.060}_{-0.067}$	$0.566^{+0.093}_{-0.106}$	–	–	–
Flat w CDM	23.865 ± 0.013	–	$0.273^{+0.070}_{-0.101}$	–	$-0.82^{+0.16}_{-0.16}$	–	–
Padé	23.866 ± 0.014	–	–	–	–	$-0.396^{+0.072}_{-0.112}$	$0.664^{+0.851}_{-0.452}$
Flat Padé	23.861 ± 0.011	–	–	–	–	-0.441 ± 0.024	–
Pantheon+							
Empirical	23.810 ± 0.006	-0.594 ± 0.023	–	–	–	–	–
Flat Λ CDM	23.807 ± 0.007	–	0.331 ± 0.018	–	–	–	–
Λ CDM	23.810 ± 0.008	–	$0.298^{+0.053}_{-0.055}$	$0.619^{+0.077}_{-0.084}$	–	–	–
Flat w CDM	23.811 ± 0.009	–	$0.293^{+0.067}_{-0.073}$	–	$-0.91^{+0.14}_{-0.17}$	–	–
Padé	23.809 ± 0.010	–	–	–	–	$-0.492^{+0.069}_{-0.111}$	$1.167^{+0.955}_{-0.502}$
Flat Padé	23.811 ± 0.007	–	–	–	–	-0.471 ± 0.026	–
Pantheon+ ($z < 1.121$)							
Empirical	23.812 ± 0.007	-0.606 ± 0.026	–	–	–	–	–
Flat Λ CDM	23.808 ± 0.007	–	0.336 ± 0.019	–	–	–	–
Λ CDM	23.810 ± 0.009	–	$0.315^{+0.082}_{-0.091}$	$0.636^{+0.107}_{-0.121}$	–	–	–
Flat w CDM	23.809 ± 0.010	–	$0.324^{+0.074}_{-0.117}$	–	$-0.97^{+0.22}_{-0.21}$	–	–
Padé	23.809 ± 0.010	–	–	–	–	$-0.505^{+0.082}_{-0.136}$	$1.323^{+1.324}_{-0.660}$
Flat Padé	23.811 ± 0.007	–	–	–	–	-0.468 ± 0.028	–


Fig. 4. Hubble diagrams of DES-SN5YR and Pantheon+, along with the best-fit $m(z)$ relations. The lower panels show the residuals relative to the empirical relation.

DES-SN5YR ($\Delta_{\text{AICc}} = 2.2$ and $\Delta_{\text{BIC}} = 2.1$). In contrast, the Λ CDM model, the flat w CDM model, and the Padé cosmography are less supported by the AICc and disfavoured by the BIC, reflecting the penalty associated with their additional free parameter.

4.4. Deceleration parameter and Hubble constant

Table 4 lists the q_0 values. For the flat Λ CDM, Λ CDM, and flat w CDM models, we used $q_0 = \Omega_M/2 + (1 + 3w)\Omega_\Lambda/2$. Although

developed solely to fit Hubble diagrams, the q_0 values of the empirical relation are consistent with those of the other $m(z)$ relations.

We estimated H_0 using the empirical relation together with Pantheon+ ($z < 1.121$) and the Cepheid distance moduli (μ_{Ceph}) from the SH0ES sample (Riess et al. 2022). To do this, we replaced Eq. (10) with $\Delta m_i = m_i - M - \mu_{\text{Ceph},i}$ for those SNe hosted in galaxies with μ_{Ceph} . We obtain $M = -19.244 \pm 0.030$, $b = -0.604 \pm 0.026$, and $H_0 = 73.4 \pm 1.0 \text{ km s}^{-1} \text{ Mpc}^{-1}$. This H_0 value is consistent with those obtained by Brout et al. (2022)

Table 3. AICc and BIC statistics.

Relation	χ^2_{\min}	AICc	BIC	Δ_{AICc}	Δ_{BIC}
DES-SN5YR					
Empirical	1638.1	1642.1	1653.2	0.0	0.0
Flat Λ CDM	1640.3	1644.3	1655.3	2.2	2.1
Λ CDM	1639.5	1645.5	1662.1	3.4	8.9
Flat w CDM	1639.0	1645.0	1661.5	2.9	8.3
Padé	1639.4	1645.4	1662.0	3.3	8.8
Flat Padé	1639.7	1643.7	1654.7	1.6	1.5
Pantheon+ ($z < 1.121$)					
Empirical	1392.3	1396.3	1407.0	0.6	0.5
Flat Λ CDM	1391.7	1395.7	1406.5	0.0	0.0
Λ CDM	1391.7	1397.7	1413.7	2.0	7.2
Flat w CDM	1391.7	1397.7	1413.8	2.0	7.3
Padé	1391.7	1397.7	1413.7	2.0	7.2
Flat Padé	1391.8	1395.8	1406.5	0.1	0.0

Table 4. Values of q_0 for different magnitude–redshift relations.

Relation	DES-SN5YR	Pantheon+ ($z < 1.121$)
	q_0	q_0
Empirical	$-0.422^{+0.019}_{-0.019}$	$-0.442^{+0.024}_{-0.024}$
Flat Λ CDM	$-0.475^{+0.026}_{-0.025}$	$-0.496^{+0.030}_{-0.028}$
Λ CDM	$-0.417^{+0.077}_{-0.067}$	$-0.478^{+0.081}_{-0.071}$
Flat w CDM	$-0.392^{+0.076}_{-0.074}$	$-0.483^{+0.096}_{-0.092}$
Padé	$-0.396^{+0.072}_{-0.112}$	$-0.505^{+0.082}_{-0.136}$
Flat Padé	$-0.441^{+0.025}_{-0.023}$	$-0.468^{+0.028}_{-0.027}$

from Pantheon+ and SH0ES, which range from 73.3 ± 1.1 to $73.6 \pm 1.1 \text{ km s}^{-1} \text{ Mpc}^{-1}$.

4.5. Stability in the absence of low- z SNe

To evaluate the stability of the best-fit parameters of the six $m(z)$ relations in the absence of low- z SNe, we computed \mathcal{M} and q_0 using SNe with $z > z_{\min}$, where $z_{\min} = 0.01, 0.03, 0.06, 0.10$, and 0.15 . Fig. 5 shows the resulting (\mathcal{M}, q_0) points. We find that the empirical relation, the flat Λ CDM model, and the flat Padé model are the most stable in the absence of low- z SNe. Because the best-fit parameters of the empirical relation are the intercept and slope of the approximately linear correlation between $m - 5 \log(z(1+z))$ and z (see Fig. 2 and Eq. (11)), their stability depends primarily on the z baseline of the data. Therefore, they are expected to vary only mildly when low- z SNe are removed.

When fitted to DES-SN5YR, the three most stable relations show a gap between cases with $z_{\min} \geq 0.06$ and those with $z_{\min} \leq 0.03$. For $z_{\min} \geq 0.06$, the selection removes at least 85% of the SNe in the low- z sample of DES-SN5YR. This likely reflects differences in the low- z sample relative to the rest of DES-SN5YR, as also discussed by Huang et al. (2025). This effect does not affect the analysis of the S1, S2, S4, and S5 deep-field regions, as they do not contain any SNe from the low- z sample.

4.6. Deep-field regions

Fig. 6 shows the Hubble diagrams for the deep-field regions. To constrain the parameters of the S1, S2, S4, and S5 regions, we

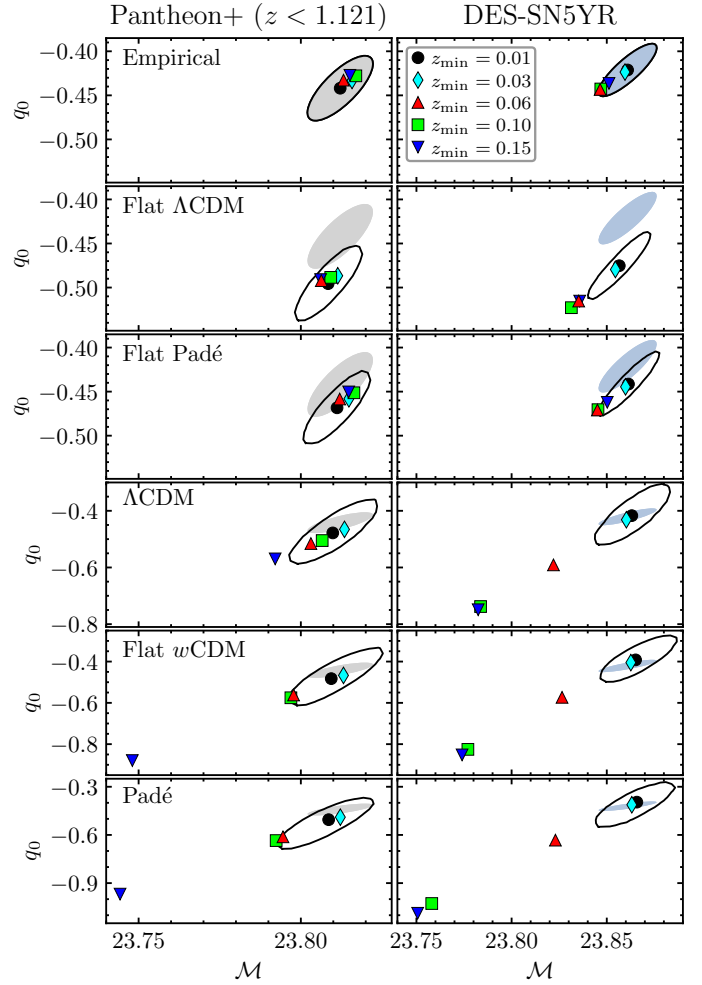


Fig. 5. Distribution of q_0 versus \mathcal{M} for the $m(z)$ relations fitted to DES-SN5YR and Pantheon+ ($z < 1.121$) with different z_{\min} . Solid curves are the 68.27% confidence contours for $z_{\min} = 0.01$, while the contour of the empirical relation is shown as a shaded region in each panel for comparison. Although the flat w CDM constraints in the (w, Ω_M) plane are highly non-Gaussian, their projection onto q_0 leads to nearly symmetric uncertainties, as expected since $q_0 = Q_H(z=0)$, where the parameter $Q_H(z)$ is almost free of the w – Ω_M degeneracy (Camilleri et al. 2024).

selected the m and z values for the SNe in these regions, along with the corresponding entries of the covariance matrix. We then replaced Eq. (10) with $\Delta m_i = m_i - m(z_i, \mathbf{v}_j)$ for the SNe within the j -th region with parameters \mathbf{v}_j . We applied the same procedure to the S367, N147, N235, and N6 regions. Table 5 lists the parameter constraints for the empirical relation, the flat Λ CDM model, and the flat Padé model. Fig. 6 shows the best fits.

Table 6 lists the Δ_{AICc} and Δ_{BIC} values for the empirical relation, the flat Λ CDM model, and the flat Padé model. These values indicate that the three $m(z)$ relations provide comparable fits to the Hubble diagrams in the deep-field regions. Since the empirical relation is purely phenomenological and its parameters, uncertainties, and confidence contours can be computed analytically (Sect. 4.1), we used it as a convenient parametrisation to characterise the deep-field regions.

Fig. 7 shows the confidence contours and the marginalised distributions for \mathcal{M} and b for the deep-field regions. The b values are consistent within 1.6σ . When accounting for the 0.04 mag offset between the selection bias corrections in DES-SN5YR and Pantheon+, the \mathcal{M} values are consistent within 1.6σ , in

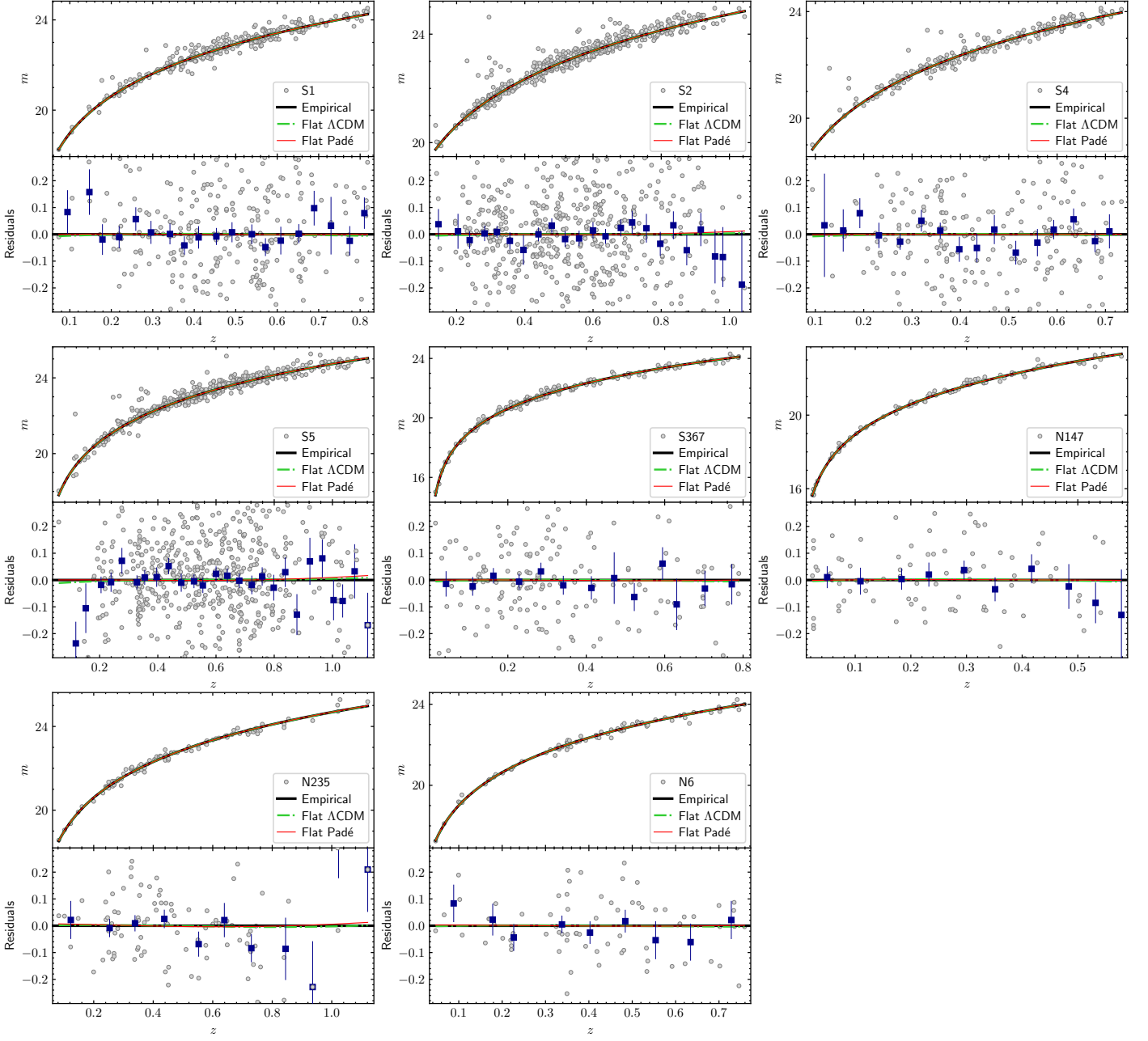


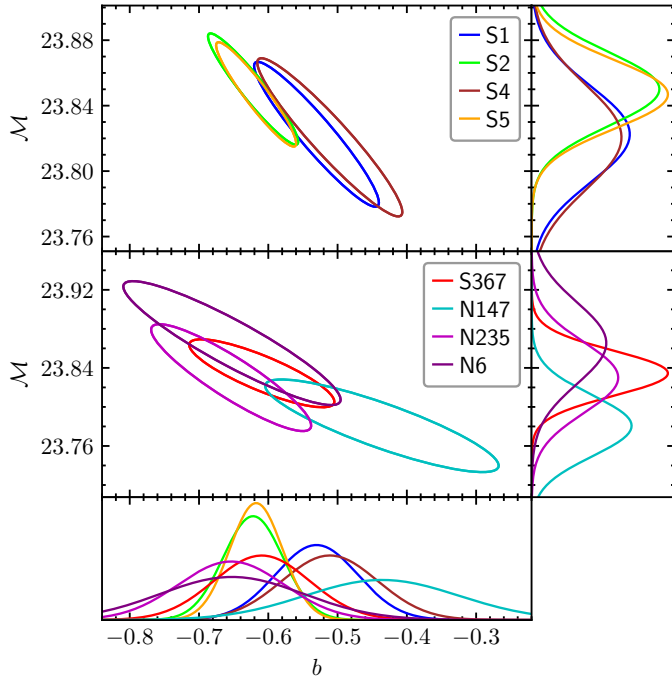
Fig. 6. Same as Fig. 4, but for the deep-field regions.

Table 5. Parameter constraints for the deep-field regions.

Region	Empirical relation		Flat Λ CDM model		Flat Padé model	
	\mathcal{M}	b	\mathcal{M}	Ω_M	\mathcal{M}	q_0
S1	23.823 ± 0.029	-0.530 ± 0.059	$23.810^{+0.036}_{-0.028}$	$0.273^{+0.049}_{-0.037}$	$23.820^{+0.034}_{-0.028}$	$-0.548^{+0.070}_{-0.056}$
S2	23.850 ± 0.022	-0.622 ± 0.043	$23.837^{+0.029}_{-0.024}$	$0.333^{+0.042}_{-0.031}$	$23.851^{+0.027}_{-0.023}$	$-0.448^{+0.057}_{-0.047}$
S4	23.821 ± 0.032	-0.511 ± 0.069	$23.806^{+0.038}_{-0.030}$	$0.257^{+0.055}_{-0.040}$	$23.816^{+0.037}_{-0.031}$	$-0.571^{+0.079}_{-0.064}$
S5	23.847 ± 0.021	-0.618 ± 0.038	$23.831^{+0.027}_{-0.022}$	$0.327^{+0.036}_{-0.028}$	$23.846^{+0.025}_{-0.021}$	$-0.455^{+0.049}_{-0.041}$
S367	23.834 ± 0.023	-0.609 ± 0.069	$23.828^{+0.027}_{-0.022}$	$0.335^{+0.059}_{-0.045}$	$23.833^{+0.026}_{-0.022}$	$-0.465^{+0.083}_{-0.067}$
N147	23.781 ± 0.031	-0.436 ± 0.111	$23.775^{+0.035}_{-0.028}$	$0.227^{+0.078}_{-0.060}$	$23.778^{+0.034}_{-0.029}$	$-0.637^{+0.114}_{-0.092}$
N235	23.830 ± 0.036	-0.654 ± 0.076	$23.830^{+0.050}_{-0.038}$	$0.376^{+0.084}_{-0.056}$	$23.838^{+0.046}_{-0.037}$	$-0.397^{+0.111}_{-0.083}$
N6	23.865 ± 0.042	-0.652 ± 0.103	$23.862^{+0.055}_{-0.040}$	$0.370^{+0.103}_{-0.068}$	$23.868^{+0.051}_{-0.042}$	$-0.412^{+0.140}_{-0.103}$

Table 6. AICc and BIC statistics for the deep-field regions.

Relation	χ^2_{\min}	AICc	BIC	Δ_{AICc}	Δ_{BIC}
S367+N147+N235+N6					
Empirical	376.8	393.1	425.3	0.6	0.7
Flat Λ CDM	376.2	392.5	424.7	0.0	0.1
Flat Padé	376.1	392.5	424.6	0.0	0.0
S1+S2+S4+S5					
Empirical	1442.9	1459.0	1502.1	0.0	0.0
Flat Λ CDM	1443.9	1460.0	1503.1	1.0	1.0
Flat Padé	1444.6	1460.7	1503.8	1.7	1.7


Fig. 7. Confidence contours (68.27%) and marginalised distributions of empirical relation parameters fitted to the deep-field regions.

agreement with isotropy. We obtain similar results when comparing the parameters of the flat Λ CDM and flat Padé models, for which the differences in M , Ω_M , and q_0 do not exceed 1.7σ , 1.5σ , and 1.7σ , respectively.

To test whether fitting the S1, S2, S4, and S5 regions with different parameters for each region (eight parameters in total) provides a significantly better fit than an isotropic fit (two parameters for all regions), we performed a likelihood ratio test (LRT). The test statistic $\lambda = \chi^2_{\min, \text{iso}} - \chi^2_{\min}$, where χ^2_{\min} is the value for the model with eight parameters (listed in Table 6) and $\chi^2_{\min, \text{iso}}$ is the corresponding value for the isotropic fit, follows a χ^2 distribution with six degrees of freedom (Wilks 1938). Fitting the empirical relation, we obtain $\chi^2_{\min, \text{iso}} = 1451.3$, $\lambda = 8.4$, and a p -value of 0.21. For the S367, N235, N147, and N6 regions, we find $\chi^2_{\min, \text{iso}} = 383.5$, $\lambda = 6.7$, and a p -value of 0.35. In both cases, the isotropic fit cannot be rejected. We obtain similar results when using the flat Λ CDM and flat Padé models, for which the LRT p -values lie between 0.20 and 0.36. Therefore, we find no evidence for anisotropy in the Hubble diagrams of the deep-field regions.

Table 7. Values of q_0 for deep-field regions.

Region	q_0 (Empirical)	q_0 (Flat Padé)	q_0 (Flat Λ CDM)
S1	-0.511 ± 0.055	$-0.548^{+0.070}_{-0.056}$	$-0.591^{+0.075}_{-0.055}$
S2	-0.427 ± 0.040	$-0.448^{+0.057}_{-0.047}$	$-0.500^{+0.062}_{-0.047}$
S4	-0.529 ± 0.064	$-0.571^{+0.079}_{-0.064}$	$-0.615^{+0.083}_{-0.060}$
S5	-0.431 ± 0.035	$-0.455^{+0.049}_{-0.041}$	$-0.510^{+0.055}_{-0.041}$
S367	-0.439 ± 0.064	$-0.465^{+0.083}_{-0.067}$	$-0.497^{+0.089}_{-0.067}$
N147	-0.598 ± 0.102	$-0.637^{+0.114}_{-0.092}$	$-0.660^{+0.117}_{-0.089}$
N235	-0.398 ± 0.070	$-0.397^{+0.111}_{-0.083}$	$-0.436^{+0.126}_{-0.084}$
N6	-0.399 ± 0.095	$-0.412^{+0.140}_{-0.103}$	$-0.445^{+0.154}_{-0.103}$

Table 7 lists the q_0 values for the deep-field regions. The values measured using the empirical relation are consistent within 1.6σ and are lower than zero by more than 4.8σ (99.9998% confidence). These results indicate that the Universe is undergoing accelerated expansion in a statistically consistent manner across all eight deep-field regions, under the assumption that the large-scale densities in these regions are independent of the comoving radial coordinate.

4.7. Application to other samples

4.7.1. DES-Dovekie sample

As this work was nearing completion, Popovic et al. (2025) presented a re-analysis of DES-SN5YR. The resulting recalibrated dataset, DES-Dovekie³, includes improved photometric cross-calibration and a fixed host-galaxy colour law. Since DES-Dovekie supersedes DES-SN5YR (Popovic et al. 2025), its analysis provides the best constraints and overall results from DES-SN combined with a low- z sample.

We fit the empirical relation ($b = -0.603 \pm 0.020$), Padé cosmography ($q_0 = -0.444^{+0.072}_{-0.114}$, $\hat{f}_0 = 0.805^{+0.881}_{-0.466}$), flat Λ CDM ($\Omega_M = 0.329 \pm 0.015$), Λ CDM ($\Omega_M = 0.286^{+0.056}_{-0.062}$, $\Omega_\Lambda = 0.600^{+0.088}_{-0.102}$ or $\Omega_k = 0.11^{+0.16}_{-0.14}$), flat w CDM ($\Omega_M = 0.268^{+0.063}_{-0.086}$, $w = -0.85 \pm 0.15$), and the flat Padé model ($q_0 = -0.470 \pm 0.022$). The parameters are consistent with those derived from DES-SN5YR and Pantheon+ ($z < 1.121$), as well as with those reported by Popovic et al. (2025) for the flat Λ CDM ($\Omega_M = 0.330 \pm 0.015$), Λ CDM ($\Omega_M = 0.279 \pm 0.057$, $\Omega_k = 0.14 \pm 0.15$), and flat w CDM models ($\Omega_M = 0.263^{+0.064}_{-0.078}$, $w = -0.838^{+0.130}_{-0.142}$). The Δ_{AICc} and Δ_{BIC} values are similar to those obtained for DES-SN5YR.

The magnitude differences between a flat Λ CDM model with Ω_M from Planck CMB measurements ($\Omega_M^{\text{Planck}} = 0.3166$; Planck Collaboration VI 2020) and the empirical relation have rms = 0.004 mag and a maximum absolute deviation $\Delta m_{\text{max}} = 0.011$ mag. In comparison, the empirical relation calibrated with DES-SN5YR and Pantheon+ ($z < 1.121$) yields (rms, Δm_{max}) = (0.012, 0.025) for DES-SN5YR and (0.008, 0.014) for Pantheon+. Hence, the empirical relation shows close agreement with the flat Λ CDM model using Ω_M^{Planck} , particularly when calibrated using DES-Dovekie and Pantheon+ ($z < 1.121$).

For the S1, S2, S4, and S5 regions in DES-Dovekie, the b values are -0.555 ± 0.058 , -0.612 ± 0.040 , -0.474 ± 0.066 , and -0.585 ± 0.036 , respectively. These values and those from S367, N147, N235, and N6 are mutually consistent within 1.8σ . Using

³ <https://github.com/des-science/DES-SN5YR>

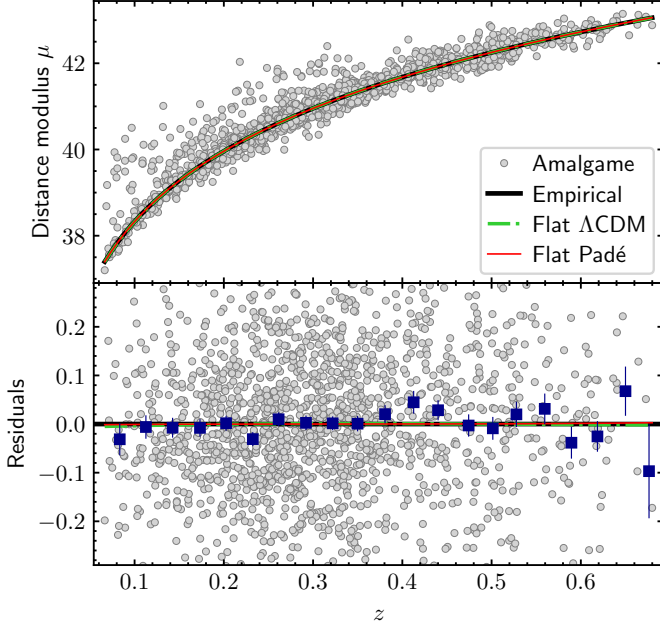


Fig. 8. Same as Fig. 4, but for the Amalgame SN sample.

an LRT, we obtain $\lambda = 6.6$ and a p -value of 0.36, indicating that the isotropic fit cannot be rejected. The corresponding q_0 values for S1, S2, S4, and S5 regions are -0.489 ± 0.054 , -0.436 ± 0.037 , -0.564 ± 0.061 , and -0.461 ± 0.033 , respectively.

We also constrained parameters using only DES SNe within DES-Dovekie. For this, we selected SNe with $z > 0.093$, thereby excluding the low- z sample entirely. We obtain $b = -0.589 \pm 0.026$ for the empirical relation, $\Omega_M = 0.307 \pm 0.020$ for the flat Λ CDM model, and $q_0 = -0.488 \pm 0.029$ for the flat Padé model. The corresponding Δ IC values are 0.5, 0.0, and 2.1, indicating that the empirical relation and the flat Λ CDM model provide comparable fits to the Hubble diagram.

4.7.2. Amalgame sample

The Amalgame sample (Popovic et al. 2024)⁴ consists of 1792 photometrically classified SNe Ia from the Sloan Digital Sky Survey (Sako et al. 2011) and Pan-STARRS1 (Scolnic et al. 2018), spanning $0.066 < z < 0.680$. We obtain $b = -0.613 \pm 0.041$ for the empirical relation, $\Omega_m = 0.334^{+0.031}_{-0.027}$ for the flat Λ CDM model, and $q_0 = -0.469^{+0.045}_{-0.041}$ for the flat Padé model. These values are consistent with values obtained from Pantheon+ ($z < 1.121$), DES-SN5YR, and DES-Dovekie. Fig. 8 shows the Hubble diagram for Amalgame. The Δ IC values for the empirical relation, the flat Λ CDM model, and the flat Padé model are 0.4, 0.0, and 0.6, respectively, showing that all three provide comparable fits to the Hubble diagram.

4.7.3. Baryon acoustic oscillation distances and cosmic chronometers

Although the empirical relation is designed to fit Hubble diagrams of standard candles, we applied it to available $d_M(z)$ and $H(z)$ datasets assuming the FLRW metric, which allowed us to transform the empirical relation into expressions for $d_M(z)$ (Eq. 13) and $H(z)$ (Eq. 14).

Abdul Karim et al. (2025) reported 13 distance measurements from baryon acoustic oscillations (BAO) in the second

Table 8. Values of \hat{j}_0 for different magnitude–redshift relations.

Relation	Pantheon+ ($z < 1.121$)	DES-SN5YR
	\hat{j}_0	\hat{j}_0
Empirical	$0.585^{+0.014}_{-0.011}$	$0.596^{+0.012}_{-0.011}$
Λ CDM	$0.902^{+0.371}_{-0.415}$	$0.726^{+0.298}_{-0.339}$
Flat w CDM	$0.909^{+0.672}_{-0.575}$	$0.514^{+0.409}_{-0.345}$
Padé	$1.323^{+1.324}_{-0.660}$	$0.664^{+0.851}_{-0.452}$

data release (DR2) of the Dark Energy Spectroscopic Instrument (DESI), relative to the sound horizon (r_d), at effective redshifts z_{eff} ranging from 0.295 to 2.33⁵. These include six $d_M(z)/r_d$ values, six $d_H(z)/r_d$ values (with $d_H(z) = c/H(z)$), and one $d_V(z)/r_d$ value, where $d_V(z) \equiv [z d_M(z)^2 d_H(z)]^{1/3}$. Fitting Eqs. (13) and (14) to the seven BAO distances with $z_{\text{eff}} < 1.121$, and assuming $\Omega_k = 0$, we obtain $b = -0.584 \pm 0.016$. For comparison, the b values obtained from Pantheon+ ($z < 1.121$), DES-SN5YR, DES-Dovekie, and Amalgame, when all SN samples are restricted to $z \geq 0.295$, are -0.697 ± 0.050 , -0.622 ± 0.035 , -0.618 ± 0.033 , and -0.688 ± 0.070 , respectively. Compared to the BAO constraint, the latter three values are consistent within 1.4σ , while the Pantheon+ ($z < 1.121$) result is marginally consistent, showing a 2.2σ difference.

Alfano et al. (2026) collected 34 $H(z)$ values measured with cosmic chronometers, spanning $0.07 \leq z \leq 1.965$. Fitting Eq. (14) to the 27 $H(z)$ values with $z < 1.121$, and assuming $\Omega_k = 0$, we obtain $b = -0.635 \pm 0.095$. This value is consistent with those from Pantheon+ ($z < 1.121$), DES-SN5YR, DES-Dovekie, and Amalgame when all SN samples are restricted to $z \geq 0.07$, yielding $b = -0.617 \pm 0.033$, -0.607 ± 0.027 , -0.591 ± 0.024 , and -0.613 ± 0.041 , respectively.

5. Discussion

5.1. Jerk parameter

The value of j_0 provides an observational test for the flat Λ CDM model (Bochner et al. 2015). Indeed, for the non-flat w CDM model (Eq. 4), Eq. (6) yields $j_0 = 1 - \Omega_k + 3(1+w)(2q_0 + \Omega_k - 1)/2$, which reduces to $j_0 = 1$ for the flat Λ CDM model. Therefore, if j_0 deviates from unity, it could indicate that the Universe is not flat, that dark energy is not a cosmological constant, or that Eq. (4) is incorrect. Given that $\hat{j}_0 = 1$ for the flat Λ CDM model, the test remains valid if \hat{j}_0 is used instead of j_0 .

Table 8 lists the \hat{j}_0 values. For the empirical relation, we use

$$\hat{j}_0 = \frac{9}{4} \left(\frac{5}{9} + q_0 \right)^2 + \frac{5}{9}, \quad (16)$$

which is derived from Eqs. (6) and (14). For DES-SN5YR and Pantheon+ ($z < 1.121$), the \hat{j}_0 values are consistent within 1.2σ . In particular, the \hat{j}_0 values for the Λ CDM model, the flat w CDM model, and the Padé cosmography are consistent with unity within 1.2σ . In contrast, the \hat{j}_0 values for the empirical relation are approximately 0.4 below unity, with an overwhelming significance of at least 30σ . Assuming $w = -1$, these values translate to $\Omega_k = 0.208^{+0.005}_{-0.007}$ and $0.202^{+0.005}_{-0.006}$ for Pantheon+ ($z < 1.121$) and DES-SN5YR, respectively; or, assuming $\Omega_k = 0$, to $w = -0.853 \pm 0.001$ and -0.854 ± 0.001 , respectively.

⁵ Data are available at https://github.com/CobayaSampler/bao_data/tree/master/desi_bao_dr2

⁴ <https://github.com/bap37/AmalgameDR>

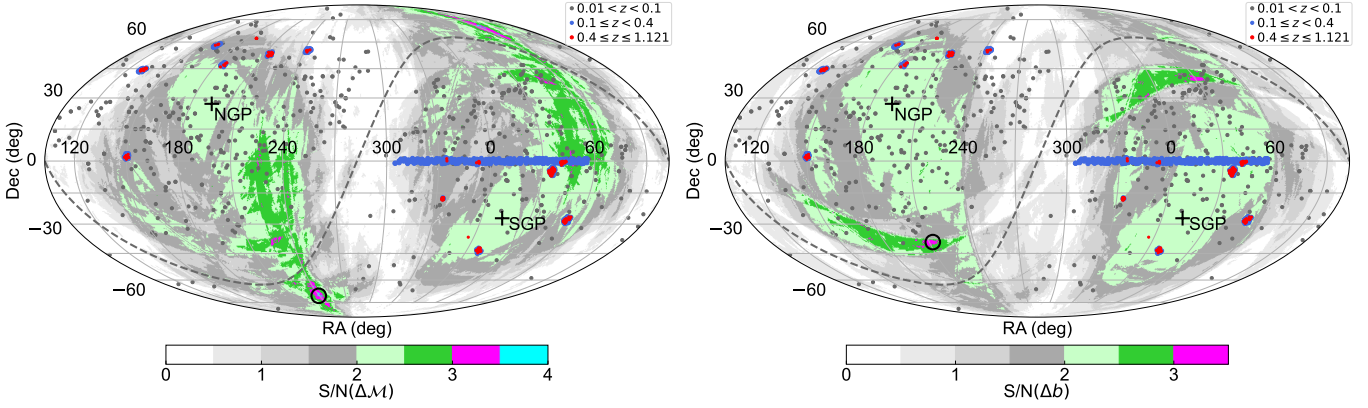


Fig. 9. Sky maps of $S/N(\Delta M)$ and $S/N(\Delta b)$. Dots represent the SNe in Pantheon+ ($z < 1.121$) and circles mark the maximum S/N values.

However, the empirical relation is intended to fit the Hubble diagram, not its derivatives. Therefore, although the empirical relation provides q_0 values consistent with those from other $m(z)$ relations (see Table 4), it may misestimate \hat{f}_0 .

5.2. Cosmic anisotropies through hemisphere comparison

Pantheon+ has been widely used to search for anisotropies in cosmological parameters using the hemisphere comparison (HC) method (Schwarz & Weinhorst 2007) under different cosmological models (e.g. Mc Conville & Colgáin 2023; Clocchiatti et al. 2024; Hu et al. 2024a,b). The HC method splits the sky into two opposite hemispheres (‘up’ and ‘down’), constrains the cosmological parameter x in each, computes a statistic such as the signal-to-noise ratio (S/N) of $\Delta x = |x_{\text{up}} - x_{\text{down}}|$, and repeats the procedure for different directions across the sky.

We applied the HC method to Pantheon+ ($z < 1.121$) using the empirical relation. We selected a set of directions on the celestial sphere using HEALPY (Górski et al. 2005; Zonca et al. 2019) with a grid resolution parameter $N_{\text{side}} = 128$. This provided 196.608 equal-area pixels on the sky, corresponding to a set of 98.304 independent directions. For each direction, we computed $S/N(\Delta x) = \Delta x / (\sigma_{\text{up}}^2 + \sigma_{\text{down}}^2 - 2\sigma_{\text{up,down}})^{1/2}$, where σ_{up} and σ_{down} are the uncertainties of x_{up} and x_{down} , respectively, and $\sigma_{\text{up,down}}$ is their covariance. Fig. 9 shows the sky maps of $S/N(\Delta M)$ and $S/N(\Delta b)$. Their maximum values are 3.7 at (RA, Dec) = (239.2°, -70.17°) and 3.3 at (RA, Dec) = (212.3°, -39.07°), respectively.

To evaluate the probabilities of obtaining $S/N(\Delta M) \geq 3.7$ and $S/N(\Delta b) \geq 3.3$ by chance when scanning many directions on the sky (the look-elsewhere effect; Bayer & Seljak 2020), we performed 10^4 simulations. In each simulation, we randomised the RA and Dec coordinates of the SNe and produced the $S/N(\Delta M)$ and $S/N(\Delta b)$ maps using the HC method and the same directions as above. The probabilities of obtaining $S/N(\Delta M) \geq 3.7$ and $S/N(\Delta b) \geq 3.3$ by chance are 6.0% and 11.2%, respectively, corresponding to 1.9σ and 1.6σ significances. Therefore, we find no evidence for anisotropies in M and b .

If the directions of maximum $S/N(\Delta M)$ and $S/N(\Delta b)$ were real anisotropies, detecting them at a 3σ level with the HC method would require adding 2500 and 4400 SNe to Pantheon+ ($z < 1.121$), respectively. An alternative approach would be to perform deep-field SN surveys towards the directions of the candidate anisotropies. This is particularly important given the absence of high- z SNe near those directions (see Fig. 9).

5.3. JWST, LSST, CSST, and Roman

Given the small number of SNe at $z > 1.121$, the validity of the empirical relation beyond this redshift remains to be verified. At present, the James Webb Space Telescope (JWST) is observing SNe Ia at $z > 1.7$ (Casey et al. 2023; DeCoursey et al. 2025). Siebert et al. (2025) report $\mu = 46.08^{+0.19}_{-0.18}$ for SN 2025ogs at $z = 2.05$, while Piel et al. (2025) report $\mu = 46.10^{+0.17}_{-0.18}$ for SN 2023aeax at $z = 2.15$ and $\mu = 47.14^{+0.21}_{-0.24}$ for SN 2023adsy at $z = 2.903$. At these redshifts, adopting the parameters inferred from Pantheon+ (Table 2) and $H_0 = 70 \text{ km s}^{-1} \text{ Mpc}^{-1}$, the empirical relation predicts $\mu = 45.92, 46.04,$ and 46.71 , whereas the Λ CDM model predicts $\mu = 46.0, 46.13,$ and 46.94 , respectively. The μ values for SNe 2025ogs and 2023aeax are consistent with both relations, whereas that for SN 2023adsy is more consistent with the Λ CDM model than with the empirical relation. However, due to its red colour, it is uncertain whether SN 2023adsy is representative of high- z SNe Ia or an outlier (Piel et al. 2024, 2025).

Beyond JWST, future deep-field surveys with the China Space Station Telescope (CSST; Li et al. 2023) and the Nancy Grace Roman Space Telescope (Hounsell et al. 2023) will observe SNe Ia up to $z = 1.3$ and $z = 1.7$, respectively. These SNe, combined with those observed by JWST and the 19 SNe at $1.121 < z \leq 2.261$ in Pantheon+, will be essential for determining the maximum z at which the empirical relation remains valid.

The deep rolling surveys of the Vera C. Rubin Observatory Legacy Survey of Space and Time (LSST; Gris et al. 2024) will provide photometry of thousands of SNe Ia with $z \lesssim 1.1$. Thus, the Hubble diagram for each of the five LSST Deep Drilling Fields can be analysed with the empirical relation. Of these fields, the newly defined Euclid Deep Field South (RA = 61.241°, Dec = -48.423°), located at an angular separation of 21° from the S5 field, will enable study of cosmic acceleration in a direction distinct from those analysed here.

6. Conclusions

We present a new empirical $m(z)$ relation based on data from Pantheon+ and DES-SN5YR. This relation fits their Hubble diagrams with only two parameters, M and b , both of which can be computed analytically. Notably, under the FLRW metric, $b \propto q_0 + 1$.

For the DES-SN5YR and Pantheon+ Hubble diagrams, the empirical relation provides fits up to $z = 1.121$ that closely match

those obtained with the Padé cosmography and the Λ CDM, flat Λ CDM, flat w CDM, and flat Padé models. The validity of the empirical relation beyond $z = 1.121$ cannot be reliably assessed given the small number of SNe at $z > 1.121$. Based on the Δ_{1C} values, the empirical relation performs better than the Λ CDM model, the flat w CDM model, and the Padé cosmography, and comparably to the flat Λ CDM and flat Padé models.

For DES-SN5YR and Pantheon+ ($z < 1.121$), we obtain $b = -0.628 \pm 0.021$ and $b = -0.606 \pm 0.026$, respectively. We also applied the empirical relation to DES-Dovekie and Amalgame, obtaining $b = -0.603 \pm 0.020$ and $b = -0.613 \pm 0.041$, respectively. For Pantheon+ ($z < 1.121$) combined with SH0ES, we obtain $H_0 = 73.4 \pm 1.0 \text{ km s}^{-1} \text{ Mpc}^{-1}$.

The empirical relation, as well as the flat Λ CDM and flat Padé models, remains stable in the absence of low- z SNe. Fitting the empirical relation to the Hubble diagrams of the eight deep-field regions, we find that their fitted M and b parameters are consistent within 1.6σ , in agreement with isotropy. Applying an LRT, we find no evidence of anisotropy. This result is further supported by using the empirical relation in the HC method applied to Pantheon+ ($z < 1.121$), which finds no statistically significant evidence for anisotropies in M and b .

Furthermore, the b values from the eight deep-field regions translate to q_0 values ranging from -0.6 to -0.4 , which are consistent within 1.6σ and lower than zero at 4.8σ . These results strongly support an accelerating universe, under the assumption that the large-scale density in each deep-field region is independent of the comoving radial coordinate.

Assuming an FLRW metric, the empirical relation can also be applied to BAO distances from DESI DR2, and to $H(z)$ values from cosmic chronometers. The derived b values, assuming $\Omega_k = 0$, are largely consistent with those from DES-SN5YR, Pantheon+ ($z < 1.121$), DES-Dovekie, and Amalgame.

The empirical relation, $m(z) = M + bz + 5 \log(z(1+z))$, or equivalently $d_L(z) = \frac{cz}{H_0}(1+z)10^{bz/5}$, provides a straightforward quantitative tool for fitting Hubble diagrams of SNe Ia without requiring a low- z sample. It enables tests of basic properties of the Universe in a simplified manner, reducing the computational cost typically associated with physically motivated cosmological models. Our analysis demonstrates that the empirical relation is valid at least up to $z \approx 1.1$. Ongoing and upcoming deep SN surveys will allow us to test its validity at higher redshifts.

Acknowledgements. We acknowledge the Director of the Millennium Institute of Astrophysics (MAS), Francisco Förster, for financial assistance through ANID grant ICN12_009, and acknowledge complementary funding from ANID/FONDECYT grant 1251692. OR is supported by the Rubin-Chile Fund under grant DIA2650. We thank Felipe Asenjo and Ariel Ordenes for helpful discussions.

References

Abdul Karim, M., Aguilar, J., Ahlen, S., et al. 2025, *Phys. Rev. D*, **112**, 083515
Alfano, A. C., Cafaro, C., Capozziello, S., Luongo, O., & Muccino, M. 2026, *J. High Energy Astrophys.*, **49**, 100444

Baker, G. A., & Graves-Morris, P. 1996, *Padé approximants* (Cambridge, UK: Cambridge University Press)
Bayer, A. E., & Seljak, U. 2020, *JCAP*, **2020**, 009
Bochner, B., Pappas, D., & Dong, M. 2015, *ApJ*, **814**, 7
Brout, D., Scolnic, D., Popovic, B., et al. 2022, *ApJ*, **938**, 110
Burnham, K. P., & Anderson, D. R. 2002, *Model selection and multimodel inference: a practical information-theoretic approach* (New York: Springer-Verlag)
Camilleri, R., Davis, T. M., Vincenzi, M., et al. 2024, *MNRAS*, **533**, 2615
Capozziello, S., D'Agostino, R., & Luongo, O. 2020, *MNRAS*, **494**, 2576
Casey, C. M., Kartaltepe, J. S., Drakos, N. E., et al. 2023, *ApJ*, **954**, 31
Cattoën, C., & Visser, M. 2007, *Class. Quantum Gravity*, **24**, 5985
Clocchiatti, A., Rodríguez, Ó., Ordenes Morales, A., & Cuevas-Tapia, B. 2024, *ApJ*, **971**, 19
Conley, A., Guy, J., Sullivan, M., et al. 2011, *ApJS*, **192**, 1
DeCoursey, C., Egami, E., Pierel, J. D. R., et al. 2025, *ApJ*, **979**, 250
Earp, S. W. F., Debattista, V. P., Macciò, A. V., et al. 2019, *MNRAS*, **488**, 5728
Efstathiou, G. 2025, *Philos. Trans. R. Soc. London Ser. A*, **383**, 20240022
Enqvist, C. 2008, *Gen. Relativ. Gravit.*, **40**, 451
Foreman-Mackey, D., Hogg, D. W., Lang, D., & Goodman, J. 2013, *PASP*, **125**, 306
Gelman, A., & Rubin, D. B. 1992, *Stat. Sci.*, **7**, 457
Górski, K. M., Hivon, E., Banday, A. J., et al. 2005, *ApJ*, **622**, 759
Gris, P., Awan, H., Becker, M. R., et al. 2024, *ApJS*, **275**, 21
Hounsell, R., Scolnic, D., Brout, D., et al. 2023, *ArXiv e-prints* [arXiv:2307.02670]
Hu, J. P., & Wang, F. Y. 2022, *A&A*, **661**, A71
Hu, J. P., Hu, J., Jia, X. D., Gao, B. Q., & Wang, F. Y. 2024a, *A&A*, **689**, A215
Hu, J. P., Wang, Y. Y., Hu, J., & Wang, F. Y. 2024b, *A&A*, **681**, A88
Huang, L., Cai, R.-G., & Wang, S.-J. 2025, *Sci. China Phys. Mech. Astron.*, **68**, 100413
Kass, R. E., & Raftery, A. E. 1995, *J. Am. Stat. Assoc.*, **90**, 773
Koyama, K. 2016, *Rep. Prog. Phys.*, **79**, 046902
Li, E.-K., Du, M., & Xu, L. 2020, *MNRAS*, **491**, 4960
Li, S.-Y., Li, Y.-L., Zhang, T., et al. 2023, *Sci. China Phys. Mech. Astron.*, **66**, 229511
Linder, E. V. 2006, *Phys. Rev. D*, **74**, 103518
Mc Conville, R., Colgáin, Ó., & E., 2023, *Phys. Rev. D*, **108**, 123533
Odintsov, S. D., Sáez-Chillón Gómez, D., & Sharov, G. S. 2025, *Eur. Phys. J. C*, **85**, 298
Perivolaropoulos, L., & Skara, F. 2022, *New Astron. Rev.*, **95**, 101659
Perlmutter, S., Aldering, G., Goldhaber, G., et al. 1999, *ApJ*, **517**, 565
Pierel, J. D. R., Engesser, M., Coulter, D. A., et al. 2024, *ApJ*, **971**, L32
Pierel, J. D. R., Coulter, D. A., Siebert, M. R., et al. 2025, *ApJ*, **981**, L9
Planck Collaboration VI. 2020, *A&A*, **641**, A6
Popovic, B., Scolnic, D., Vincenzi, M., et al. 2024, *MNRAS*, **529**, 2100
Popovic, B., Shah, P., Kenworthy, W. D., et al. 2025, *ArXiv e-prints* [arXiv:2511.07517]
Räsänen, S. 2006, *JCAP*, **2006**, 003
Riess, A. G., Filippenko, A. V., Challis, P., et al. 1998, *AJ*, **116**, 1009
Riess, A. G., Yuan, W., Macri, L. M., et al. 2022, *ApJ*, **934**, L7
Sako, M., Bassett, B., Connolly, B., et al. 2011, *ApJ*, **738**, 162
Sánchez, B. O., Brout, D., Vincenzi, M., et al. 2024, *ApJ*, **975**, 5
Schwarz, G. 1978, *Ann. Stat.*, **6**, 461
Schwarz, D. J., & Weinhorst, B. 2007, *A&A*, **474**, 717
Scolnic, D. M., Jones, D. O., Rest, A., et al. 2018, *ApJ*, **859**, 101
Siebert, M. R., Pierel, J. D. R., Engesser, M., et al. 2025, *ArXiv e-prints* [arXiv:2512.19783]
Sugiura, N. 1978, *Commun. Stat. Theory Methods*, **7**, 13
Vincenzi, M., Kessler, R., Shah, P., et al. 2025, *MNRAS*, **541**, 2585
Weinberg, D. H., Mortonson, M. J., Eisenstein, D. J., et al. 2013, *Phys. Rep.*, **530**, 87
Wilks, S. S. 1938, *Ann. Math. Stat.*, **9**, 60
Wiltshire, D. L. 2009, *Phys. Rev. D*, **80**, 123512
Zonca, A., Singer, L., Lenz, D., et al. 2019, *J. Open Source Software*, **4**, 1298